



## Effect of flow dynamics on a rotary wick cooler

Sampath Suranjan Salins<sup>a</sup>, H.K. Sachidananda<sup>a</sup>, Abdulla Abdul Jaleel<sup>a</sup>,  
Moin Alam<sup>a</sup>, Jaya Jatin Bhavesh Podugu<sup>a</sup>, Shiva Kumar<sup>b,\*</sup> , Sawan Shetty<sup>b</sup> 

<sup>a</sup> Manipal Academy of Higher Education, Dubai Campus, PO 345050, United Arab Emirates

<sup>b</sup> Department of Mechanical and Industrial Engineering, Manipal Institute of Technology, Manipal Academy of Higher Education, Manipal, 576104, India

### ARTICLE INFO

#### Keywords:

Evaporative cooling  
Wick  
Humidifier  
Static and dynamic  
Heat and mass transfer

### ABSTRACT

This study focuses on design & construction of rotary wick-type evaporative cooler unit, to compare humidification performance under static and dynamic conditions. The humidification process utilizes a wick, that is soaked through both gravity and capillary action. Experiments were conducted by varying the air Reynolds number from 12,223 to 61,114, motor speed from 30 to 90 rpm, and flow rate of water from 0.2 to 0.8 L per minute. The empirical results showed maximum values for temperature drop of 4 °C, specific humidity drop of 1.2 g/kg, coefficient of performance (COP) 5.65, mass transfer coefficient (MTC) 12.54 kg/m<sup>2</sup>-s, sensible heat ratio (SHR) 0.47, and latent heat ratio (LHR) 0.57. The optimal performance was achieved at a motor speed of 70 rpm and water flow rate (WFR) of 0.6 L per minute (LPM) or  $1 \times 10^{-5}$  m<sup>3</sup>/s. When comparing stationary and dynamic wick humidifier units, the dynamic unit demonstrated significantly higher performance with more uniform wettability.

### 1. Introduction

Evaporative cooling is the most cost-effective & sustainable cooling methods. It works by converting the sensible heat of air into latent heat to enhance evaporation [1]. This technology is widely used in developing countries and tropical regions. Unlike earlier systems that relied on vapor compression refrigeration (VCR), which consumed more energy and negatively impacted the environment, evaporative cooling offers a more energy-efficient alternative [2,3]. VCR-based air conditioning (AC) units account for 20 % of global power consumption, but with evaporative cooling, overall energy usage can be reduced [4,5]. The efficiency of an evaporative cooling unit depends on several factors, including inlet conditions, packing type, wettability, packing position, thickness, water flow rate, material type, and fluid flow direction [6–8]. Common packing materials include cellulose, Aspen, and Khush. Wick, a popular packing material, provides a large surface area and enhances heat and mass transfer through capillary action. Advantages of using wick include durability, corrosion resistance, refractoriness, lightweight, good water retention, and resistance to mold. Wick is typically available in strips, mats, or sheets [9,10]. Current research on evaporative cooling systems often focuses on wick as a medium, which operates effectively in both static and dynamic conditions.

Several researchers have studied various types of dynamic humidifier units. Pandelidis et al. [11] focused on Rotary Indirect Evaporative Cooler (RIEC) & compared its performance with Counter-flow Indirect Evaporative Cooler (CIEC). The study found that the RIEC obtained a 63 % upper energy efficiency ratio and was more compact. Choi et al. [12] developed a rotating evaporator cooling

\* Corresponding author.

E-mail address: [shiva.kumar@manipal.edu](mailto:shiva.kumar@manipal.edu) (S. Kumar).

unit powered by solar and wind energy, which provided 12.2 times more cooling than a conventional static unit. Salins et al. [13] built a centrifugal humidifier with a rotating cylindrical mesh that disperses water using centrifugal force. The results showed that dynamic packing obtained thermal comfort conditions more effectively than static, with the system reaching a high COP of 5.85. Kumar et al. [14] fabricated a novel multistage reciprocating humidifier unit with four packings positioned at different points. The multistage packing system outperformed the single-stage humidifier, achieving a humidification efficiency of 72.6 %. This unit also saved 7 % energy compared to a conventional VCR-based cooling unit. Yuan et al. [15] designed a ring-shaped and triangular mesh packing for efficient liquid dispersion and aggregation in a rotary humidifier. The results indicated that modified packing configuration enhanced humidification efficiency. Kumar et al. [16] operated the evaporative cooling unit at 800 rpm with an inlet temperature of 45 °C, a flow rate of air of 0.0201 kg/s, and a water flow rate of 0.066 kg/s. Results indicated that the system gave an effectiveness of 0.48, and it was able to maintain thermal comfort inside the space. Navarro et al. [17] employed an ultrasonic mist mechanism to refine droplet distribution within a rotary humidifier unit. Their findings demonstrated that an optimal water-to-air mass flow ratio significantly enhanced cooling efficiency, thereby achieving a high coefficient of performance (COP). Kumar et al. [18] studied a 3-stage centrifugal humidifier equipped with UV filters. Experiments were conducted by changing motor speed & water flow rate. The results showed an efficiency of 88.74 % and a coefficient of performance of 6.14. The air quality exiting the unit met safety standards and was deemed safe. Kim et al. [19] explored a humidification mechanism using an ultrasonic gas atomizer with a resonance chamber. The constant supply of moisture onto the packing greatly enhanced the humidification process.

Additionally, some researchers have studied humidifiers under operating conditions such as varying air & water flow rates. Kumar et al. [20] assessed the heat & mass transfer rates of a rotary humidifier by adjusting the air flow rate, water flow rate, water inlet temperature & rotational speed. The results revealed a cooling effectiveness of 0.59 & Merkel number of 1.88 for the system. Masaeli et al. [21] used a membrane humidifier (MH) to regulate the humidity & temperature in the fuel cell. Three different types of membrane humidifiers were studied: finned, serpentine, and parallel arrangements. The results indicated that at lower flow rates, serpentine arrangement performed better. Shinde et al. [22] compared polyvinyl chloride (PVC) packing with cellulose packing, assessing the influence of air & water flow rates & inlet temperature on performance. The maximum efficiency and temperature drop achieved were 93.12 % and 16.5 °C, respectively. The results demonstrated that cellulose packing outperformed PVC packing. Harby and Al-Amri [23] analysed the energy efficiency of a split AC system utilizing evaporative cooling technology under various climates. Using corrugated paper in a wind tunnel, they assessed heat and mass transfer performance and found that a packing thickness of 100 mm provided optimal performance, reducing power consumption by 29.53 %. Abdullah et al. [24] compared the performance of Aspen and thorn tree packing materials in a humidifier unit at water flow rates ranging from 1 to 4 kg/min. The results showed that Aspen pads provided better performance. Weragoda et al. [25] developed a vertically oriented capillary-driven evaporative cooler using wick as a medium. The study considered parameters such as thickness, porosity, and arrangement of the wick. It was found that higher porosity and thickness increased thermal resistance, which in turn affected the system's efficiency. Almanea [26] utilized composite porcelain along with wood, iron & aluminium waste as packing material in an evaporative cooling unit. Experiments were conducted with airflow rates ranging from 0.25 to 0.4 kg/s, and the study found that the maximum COP and pressure drop across the pad were 2.25 and 14 N/mm<sup>2</sup>, respectively. Tripathi et al. [30] investigated the dynamic thermal performance of a novel multi-vent dry channel configuration. Using both steady-state and time-dependent methods under varying climatic conditions, the system demonstrated enhanced cooling without adding moisture to the air. Results showed outlet temperature reductions ranging from 7.8 % to 15.8 % across different cases. Increasing the channel gap from 0.021 m to 0.063 m improved the temperature drop from 9.82 °C to 12.36 °C. The highest dew point effectiveness of 87.5 % was observed with a channel gap between 0.063 m and 0.084 m, while optimal cooling capacity of 13.5 kW was achieved at a gap of 0.042–0.063 m. The system reached a coefficient of performance (COP) of 6.3. In a related study, Tripathi et al. [31] developed a solar photovoltaic-powered indirect evaporative cooling system incorporating the novel multi-vent dry channel, demonstrating its potential for energy-efficient HVAC applications. Experimental results indicated that air velocity, spray water temperature, and inlet air humidity significantly influenced system performance. The system achieved an outlet air temperature of 19.8 °C and a high COP of 6.17 under low specific humidity conditions. Singh and Kumar [32] integrated a solar still with a helical parabolic collector using nanoparticle-doped phase change materials (PCMs) to enhance desalination performance. Their system achieved a maximum productivity of 3268 ml/m<sup>2</sup>/day and an energy efficiency of 46.23 %. In another study, Singh and Kumar [33] developed a solar-powered desalination system using parabolic reflectors and nano-enhanced PCMs to improve efficiency. Their system showed a 67.19 % increase in thermal efficiency and attained an exergy efficiency of 12.29 %.

An extensive literature survey revealed that many researchers have studied various humidification systems, including Rotary Indirect Evaporative Coolers (RIEC), Counter-flow Indirect Evaporative Coolers (CIEC), centrifugal humidifiers, membrane humidifiers, multistage reciprocating units, and VCR-based humidifiers. It was found that dynamic and multistage humidifiers delivered superior performance. Some studies also examined the effects of packing thickness, air velocity (AV) & water flow rate on humidification performance, with results showing that increased packing thickness improved performance. Various packing materials, such as cellulose, PVC, aspen, and thorn packings, have been studied, with cellulose packing yielding the best results.

This study addresses key research gaps in humidification by exploring the underutilized potential of wick-based systems that leverage capillary action and evaluating the performance of dynamic (rotating) humidifiers, which remain largely unexamined under varying inlet conditions. An experimental test rig was developed using rotating wick packing at different RPMs to assess parameters such as mass transfer COP, sensible and latent heat ratios, and to compare static versus dynamic systems. The study aligns with the journal's scope by advancing energy-efficient HVAC design, enhancing indoor environmental quality, and contributing to sustainable building practices. It supports green building certification goals through improved humidity control, occupant comfort, and performance evaluation using quantifiable metrics.

## 2. Methodology of wick type rotary humidifier

Fig. 1 illustrates the principle of a rotary humidifier, where a wick serves as the humidification medium. The methodology of the rotary wick humidifier utilizes a simple, yet efficient passive evaporative process enhanced by mechanical rotation. The system features a rotating drum partially submerged in a water reservoir, with absorbent wick material wrapped around its surface. As the drum slowly turns, the wick draws water from the reservoir through capillary action. A fan or natural airflow passes over the dampened wick, facilitating evaporation and increasing the humidity of the surrounding air.

Experimental trials for a rotary wick humidifier are conducted in controlled environments to assess performance. The humidifier is placed in a test space with recorded baseline conditions such as temperature, humidity, airflow, and water level. It operates for a set period while changes in humidity are measured at intervals using sensors. Three experimental trials were conducted for each test condition, and the mean value was taken as the representative reading. The trials involved parametric variations in wick materials, rotation speeds, and fan settings to evaluate their impact on humidification efficiency. This approach ensured consistent and reliable results for performance analysis and system improvement.

In rotary wick humidifier experiments, error bars are valuable tools in graphs and data visualizations to illustrate the variability or uncertainty in measured parameters such as humidification rate, temperature, and energy consumption. These bars typically represent statistical measures like standard deviation, standard error, or confidence intervals, depending on the analysis objective. In the present work, vertical error bars have been included in the graphical representations to indicate the spread of values across three experimental trials, with the mean values used as representative data points. These error bars highlight the consistency and repeatability of the results and assist in visually comparing different experimental conditions.

The COP is calculated as a ratio of the cooling effect (CE) to the work rate of the blower, pump, and motor, as shown in equation (1). Both the cooling effect (CE) and the various work inputs are expressed in watts.

$$COP = \frac{\dot{Q}_c}{(\dot{W}_{motor} + \dot{W}_{Pump} + \dot{W}_{Blower})} \quad (1)$$

Mass transfer coefficient (MTC) is defined as the ratio of evaporation rate (ER) during humidification to the surface area of the wick in contact with air & change in the specific humidity difference.

$$K = \frac{\dot{m}_w}{A \Delta W} \quad (2)$$

Total heat transfer is given by sum of sensible and latent heat and is given by equation (3).

$$\dot{Q} = \dot{Q}_c + \dot{Q}_L \quad (3)$$

Sensible heat ratio (SHR) as given in equation (4) is defined as the ratio describing the portion of sensible heat and is given by the total sensible heat of air compared to the overall heat transfer.

$$SHR = \frac{\dot{Q}_c}{\dot{Q}} = \frac{m_a C_p \Delta T}{\dot{Q}} \quad (4)$$

The Latent heat ratio (LHR) indicates the portion of heat involved in phase changes, calculated by the ratio of latent heat to total heat transfer rate. It is given by equation (5).

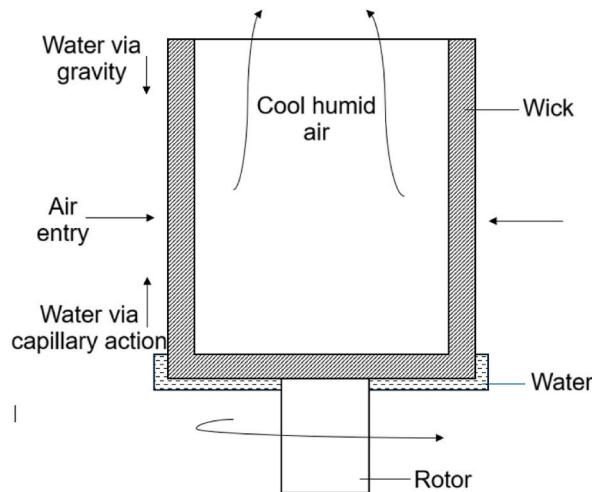


Fig. 1. Principle of wick type rotary humidifier.

$$LHR = \frac{\dot{Q}_L}{\dot{Q}} = \frac{\dot{m}_a(h_1 - h_2)}{\dot{Q}} \quad (5)$$

### 3. Construction, working and instrumentation

The rotary wick humidifier consists of key components including a high-torque motor, rotating shaft, inner and outer cylinders, wick, blower, pump, and duct, all supported by a mild steel frame. The stationary outer cylinder and rotating inner porous cylinder (powered by a 12 V, 100 RPM DC motor) are made of 1.2 mm-thick SS 304. The wick, held between the cylinders, stays moist via gravity-fed water and capillary action. A centrifugal blower (12 V, 120 W, 100 RPM) draws atmospheric air into the system. Water circulates between a main tank (for dripping onto the wick) and a collector tank, using a 5 V diaphragm pump with a 1.2 LPM flow rate. Valves, a motor shaft controller, and an airspeed controller regulate water flow, rotation speed, and airflow respectively. The duct ensures proper air distribution. Fig. 2 shows the schematic of rotary wick humidifier.

A high-torque motor, operating at low RPM, drives the rotation of the hollow inner cylinder that encases the wick. Water from the main tank is dispensed onto the wick, where it is subsequently collected in the collector tank. The wick absorbs the water through both gravitational and capillary forces. A pump then recirculates the water back to the main tank. The blower draws air through two apertures in the outer cylinder, directing it through the porous, wick-filled inner cylinder. This mechanism facilitates evaporative cooling; wherein latent heat is transformed into sensible heat. Consequently, cool, humidified air is expelled through a flexible duct and directed into the room. Fig. 3 illustrates the fully assembled rotary wick humidifier unit.

The wick is crafted from 100 % natural cotton, often combined with other materials like paper or metal cores to enhance strength and stability. It has a thickness of 3 mm and exhibits high capillary action, effectively transporting liquid due to its expansive surface area and the structure of its cotton fibres, which form small channels that facilitate upward water movement through surface tension. Its excellent water retention capacity further contributes to its performance. The wick has a density of 0.7 g/cm<sup>3</sup>, a thermal conductivity of 0.05 W/m°C, and a tensile strength of 20 MPa. Fig. 4 shows the wick covered inner frame.

Experiments on the wick-type humidifier were conducted by changing the air velocity, water flow rate & motor shaft speed. Various instruments were employed to measure the inlet & outlet parameters to assess system's performance. Air velocity was measured using an anemometer with range of 0–50 m/s, a resolution of 0.1 m/s & accuracy  $\pm 0.1$  m/s. Relative humidity (RH) was determined with a hygrometer, which has a range of 1–99 %, a resolution of 0.1 %, and an accuracy of  $\pm 0.1$  %. A digital thermometer was used to measure both dry bulb temperature (DBT) and wet bulb temperature (WBT), with a resolution of 0.1 °C, a range of 0–90 °C, and an accuracy of  $\pm 0.1$  °C. The uncertainties associated with these measurements are discussed in the following section.

### 4. Analysis of experimental uncertainty

Root Sum of Squares (RSS) is a statistical tool used to evaluate the errors in the performance parameters of the wick humidifier. Let  $Y_G$  represent the total uncertainty,  $G$  be the function,  $X$  the independent variable, and  $Y$  the uncertainty intervals. The total error is given by equation (6).

$$Y_G = \left[ \left( \frac{\partial G}{\partial X_1} Y_1 \right)^2 + \left( \frac{\partial G}{\partial X_2} Y_2 \right)^2 + \left( \frac{\partial G}{\partial X_3} Y_3 \right)^2 + \dots + \left( \frac{\partial G}{\partial X_n} Y_n \right)^2 \right]^{0.5} \quad (6)$$

The uncertainties associated with the performance parameters were calculated using Equation (6). The uncertainty calculations for all dependent variables are provided in Appendix 1. The summary of all measurement errors is provided in Table 1, while the experimental conditions are detailed in Table 2.

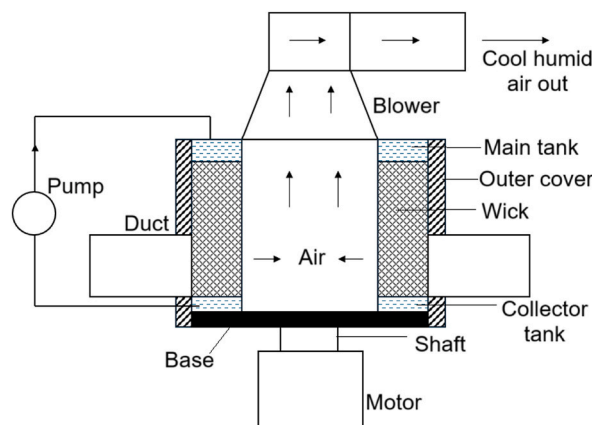


Fig. 2. Schematic diagram of Rotary Wick humidifier.

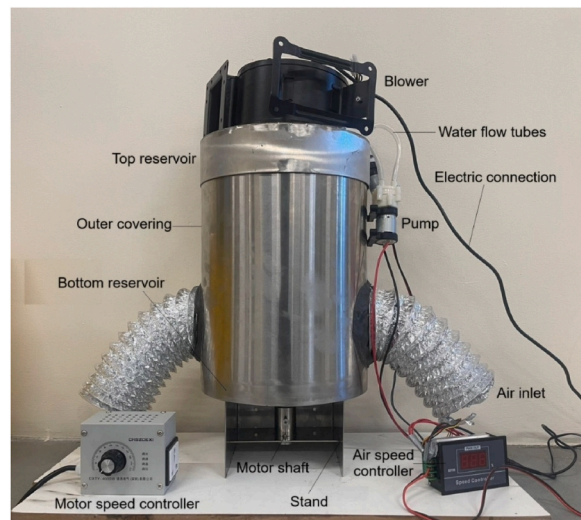


Fig. 3. Fully constructed Rotary Wick humidifier.

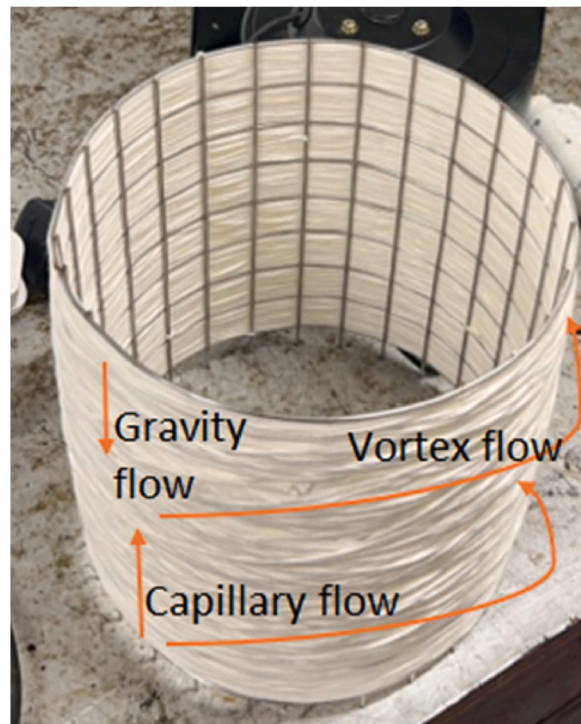


Fig. 4. Wick covered inner frame.

**Table 1**

Uncertainty or error involved in measuring rotary wick type humidification parameters.

Sl.No.	Performance parameters	Total uncertainty (%)
1.	COP	1.68
2.	Mass transfer coefficient ( $\text{kg}/\text{m}^2\text{-s}$ )	1.20
3.	Sensible heat ratio	1.59
4.	Latent heat ratio	1.38



## 5. Results & discussion

Experiments on rotary wick humidifiers are usually conducted through three separate trials to ensure the accuracy and reliability of the results. In each trial, the humidifier operates under consistent controlled conditions, such as stable temperature, airflow, and water level, while key performance metrics like humidity change, temperature variation, and power consumption are recorded. Upon completing all three trials, the collected data are averaged to reduce the impact of any anomalies or measurement errors. This averaging process yields a more reliable and representative evaluation of the humidifier's overall performance, allowing for consistent trends to be identified and the design's effectiveness to be validated. Experiments are performed by changing the air Reynolds number from 12,223 to 61,114, the flow rate of water from 0.2 to 0.8 LPM, & motor shaft speed from 30 to 90 rpm. The input & output parameters are measured to derive the performance characteristics.

This section explains the scientific basis for the observed changes in performance parameters under these input conditions. It is divided into (i) 5.1 Performance parameter variation with the air Reynold's number, flow rate of water & motor speed (ii) 5.2 Performance parameter comparison between stationary and rotating wick.

### 5.1. Impact of operational variations on key performance indicators

#### 5.1.1. Change in DBT

During the humidification process, water vapor is added to the air, increasing its moisture content and resulting in cooling. This leads to a drop in dry bulb temperature (DBT) when air meets the wick as shown in Fig. 5. At lower air velocities, interaction time between the air & water particles in the wick is longer, allowing for higher heat transfer and a greater temperature drop. As air Reynolds' number increases, the contact time between water particles in the wick and the air flowing in the crossflow direction decreases, resulting in a smaller temperature drop. In other words, air absorbs less moisture and loses less heat. At higher air velocities or Reynolds numbers, the boundary layer near the surface becomes thinner, reducing resistance to heat transfer, which diminishes the DBT drop. The change in DBT with rotating speed is determined by the interaction between the rotating wick and the air in the crossflow direction. The advantage of using the wick in dynamic conditions is that it ensures uniform wettability due to water dripping onto the wick by gravity and capillary action. As water moves up the wick, it evaporates upon contact with air, absorbing latent heat and cooling the surrounding air. Stronger capillary action transports more water for evaporation, enhancing the cooling effect and further lowering the temperature. At lower motor shaft speeds, heat and mass transfer are lower, leading to a smaller change in DBT. As the motor speed increases from 30 to 70 rpm, the wetted wick has a higher chance of meeting the air, improving heat and mass transfer. However, at speeds above 70 rpm, the wick fails to retain moisture, resulting in dryness. Splashing or inefficient distribution of water also contributes to this effect. Higher turbulence further reduces the DBT drop. As the motor shaft speed increases from 30 to 70 rpm, DBT drop increases by 14.28 %, but when the speed exceeds 70 rpm, the DBT change decreases by 5 %.

#### 5.1.2. Change in specific humidity

Fig. 6 shows the specific humidity change with Air Reynold's number and the motor shaft speed. During the humidification process, water vapor molecules diffuse into the air from the wick surface. This diffusion process occurs as water molecules move from a region of higher concentration (the wick surface) to a region of lower concentration (the air). At lower air velocities, more air molecules come into contact with the surface, allowing more water molecules to diffuse into the air, thus increasing the change in specific humidity. As air velocity increases, the boundary layer near the humidifying surface becomes thinner, which reduces the efficiency of molecular diffusion. The mass transfer coefficient, which describes the transfer of water vapor, becomes less effective due to limited contact between air & water surface, leading to smaller increase in specific humidity. At higher Reynolds numbers (turbulent flow), the diffusion process is further disrupted, minimizing the change in specific humidity. Surface tension helps water adhere to the wick, forming a thin film that supports its upward movement and consistent moisture distribution. The capillary effect enables water to travel through the wick's narrow pores, promoting continuous evaporation at the surface, which absorbs heat from the air and humidifies it. As the air Reynolds number increases from 12,223 to 61,114, the change in specific humidity decreases by 30.83 % at 0.6 LPM water flow. Varying water flow from 0.2 to 0.6 LPM increases specific humidity by 71.42 %, but beyond 0.6 LPM, it drops by 16.66 % at low Reynolds numbers. Excessive water flow limits evaporation due to pooling, reduced air-water interaction, and

**Table 2**

Experimental conditions of rotary wick type humidifier.

Sl. No.	Varying parameters a	Input & output measured values	Type of flow	Performance parameters	Type of humidification media
1.	Air Reynolds number: 12,223 to 61,114 Flow rate of water: 0.2 to 0.8 LPM Or $3.33 \times 10^{-6} \text{ m}^3/\text{s}$ to $1.33 \times 10^{-5} \text{ m}^3/\text{s}$ Motor shaft speed: 30–90 rpm.	Velocity of air, Flow rate of water, relative humidity of air, current & voltage, DBT & WBT.	Cross flow	Coefficient of performance, mass transfer coefficient, sensible heat ratio and latent heat ratio.	Wick type material.

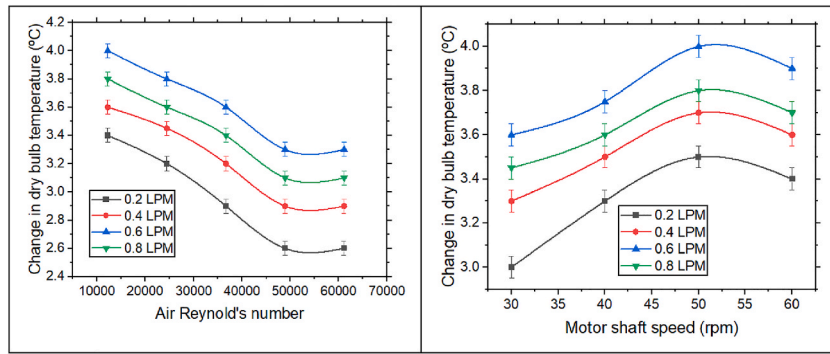


Fig. 5. Change in DBT with air Reynold's number and motor shaft speed.

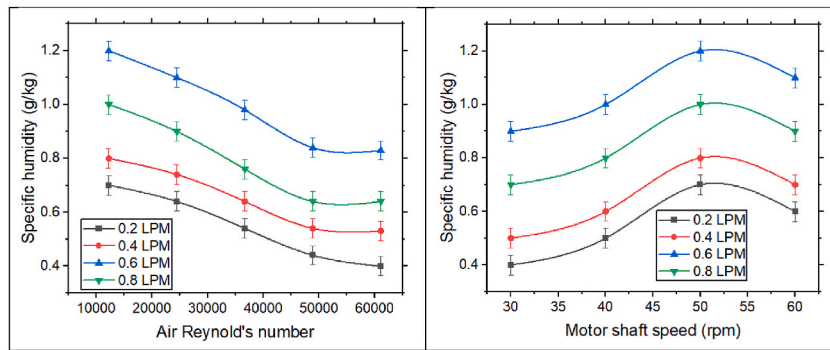


Fig. 6. Change in specific humidity with air Reynold's number and motor shaft speed.

disrupted diffusion, lowering humidification efficiency.

### 5.1.3. Coefficient of performance

The coefficient of performance (COP) is defined as the ratio of the cooling effect to the work done. As shown in Fig. 7, an increase in air velocity results in a higher COP. This improvement occurs because convective heat transfer between wick & air becomes more efficient with faster air movement. Higher air velocity converts more sensible heat into latent heat, facilitating increased evaporation. Consequently, more water molecules diffuse into the air, enhancing the mass transfer of moisture. As air velocity or Reynolds number increases, the cooling effect rises with only a modest increase in energy consumption. This increase in cooling leads to an improvement in COP. At higher air velocities, airflow transitions from laminar to turbulent, causing the air molecules to mix more chaotically, which improves the dispersion of water vapor. The turbulence increases the frequency of collisions between air and water vapor molecules, helping the water vapor spread more evenly throughout the air. Additionally, with higher air velocity, the system can better utilize the latent heat of vaporization needed to convert liquid water into vapor. The increased airflow also helps dissipate heat, preventing overheating of the humidifier surface and maintaining optimal evaporation conditions. As a result, the system becomes more efficient at transferring moisture to the air while using less energy to heat and evaporate the water. This increased efficiency leads to a higher

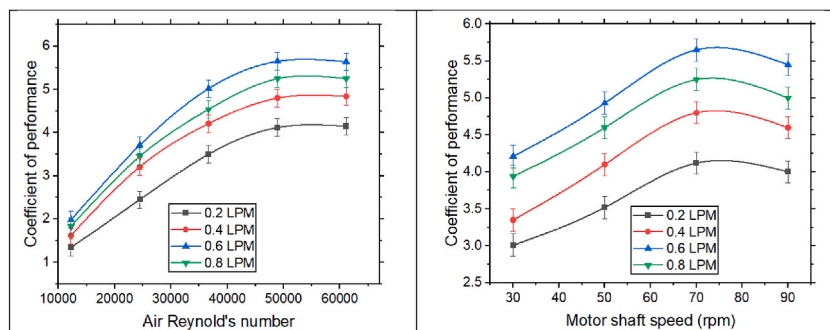


Fig. 7. Change in coefficient of performance with the air Reynold's number and motor shaft speed.

COP, with more moisture being added for the same energy input.

The rotating wick enhances air–water interaction, increasing mass transfer and improving COP. Maximum COP of 5.65 was achieved. As the air Reynolds number increased from 12,223 to 61,114 at 0.6 LPM water flow, COP rose by 184.84 %. Increasing wick speed from 30 to 70 rpm improved COP by 29.45 %, but further increase to 90 rpm led to a 3.53 % decline due to uneven wetting and reduced evaporation.

Statistical test analysis of variance (ANOVA) was conducted using experimental data collected under control conditions. Multiple trials were performed at varying Reynolds numbers and a constant water flow rate of 0.6 LPM to assess the consistency and reproducibility of the COP increase. By calculating the mean, standard deviation, and confidence intervals of the measured COP values across trials, it was possible to determine whether the observed 184.84 % increase was statistically significant. A p-value below 0.05 would confirm the significance of the improvement, reinforce the reliability of the results and support the conclusion that higher air Reynolds numbers positively influence the humidifier's performance.

#### 5.1.4. Mass transfer coefficient

The mass transfer coefficient, as shown in Fig. 8, is defined as the ratio of the evaporation rate to the product of the surface area & change in specific humidity. As the air flow rate rises, the evaporation rate correspondingly increases. This phenomenon occurs due to a rise in collision frequency between water vapor molecules & air molecules, which facilitates a more uniform distribution of water vapor throughout the air, thereby accelerating the diffusion process. The heightened flow rate induces greater turbulence, which enhances the mixing of the fluid phases. This improved mixing accelerates mass transfer, enabling water molecules to be transported more efficiently from the wick surface into the air. The enhanced vaporization is driven by absorption of sensible heat from air in contact with the wick surface. The increased turbulence further augments the diffusion of water vapor and promotes a more effective conversion of sensible heat into latent heat, thereby facilitating evaporation.

Higher rotational speeds generate intensified turbulence within the humidifier. This turbulence disrupts the boundary layers at the gas-liquid interface, reducing resistance to mass transfer and enabling a more efficient exchange of water vapor between the liquid and gas phases. Additionally, faster rotation promotes superior dispersion of liquid droplets or films, thereby expanding the effective surface area available for mass transfer. However, excessive rotation can lead to the entrainment or carryover of liquid droplets into the gas stream, depriving them of sufficient time for evaporation or absorption. This diminishes the effective interaction between the phases, consequently reducing mass transfer efficiency. At extremely high rotational speeds, centrifugal forces may cause an uneven distribution of liquid across the packing material, resulting in dry zones or areas with insufficient liquid coverage. This ultimately reduces the total surface area available for mass transfer. Moreover, excessive rotation can induce foaming or splashing of the liquid, which disrupts the stability of gas-liquid interface and compromises the effectiveness of mass transfer. The maximum mass transfer coefficient provided by the unit is 12.54 kg/m<sup>2</sup>·s.

#### 5.1.5. Sensible and latent heat ratio

The sensible heat ratio (SHR), as illustrated in Fig. 9, is given as a ratio of sensible heat to total heat. Sensible heat is calculated as product of the air flow rate, specific heat & change in temperature. As air's Reynolds number increases, the sensible heat diminishes due to a drop in temperature differential. A higher air flow rate amplifies the latent heat component. At lower air velocities, the thicker boundary layer acts as an insulating barrier, increasing thermal resistance and hindering efficient heat transfer from the wick's surface. In this scenario, the temperature change is more pronounced, allowing greater heat transfer to the air and resulting in higher sensible heat. Conversely, as air velocity rises, boundary layer thins due to the onset of turbulent flow. While this reduction in boundary layer thickness decreases thermal resistance, the faster-moving air spends less time in contact with the surface, limiting its ability to absorb sensible heat. Thus, despite the lower boundary layer resistance, the reduced contact time leads to diminished sensible heat absorption. As the Reynolds' number increases from 12,223 to 61,114, there is a reduction in the sensible heat ratio by 6.38 %. As the motor shaft speed increases, the fan or impeller rotates at a higher velocity, enhancing the airflow within the system. This increased airflow causes a greater volume of air to pass over the heat exchange surfaces, facilitating more efficient heat transfer to the air. Consequently, the sensible heat of the air rises, leading to an increase in air temperature while maintaining constant moisture. As air flows more swiftly

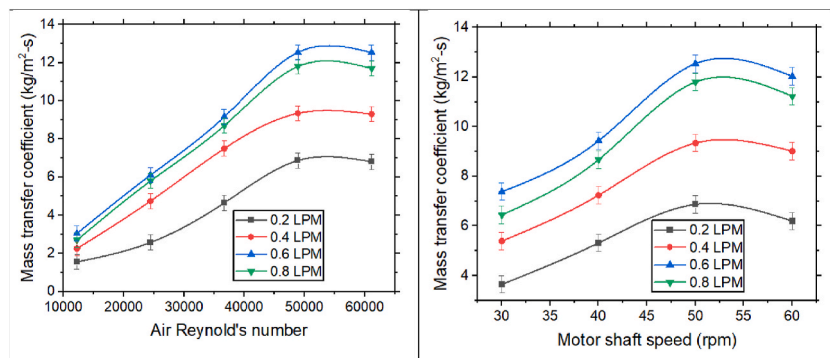


Fig. 8. Change in mass transfer coefficient with air Reynold's number & motor shaft speed.



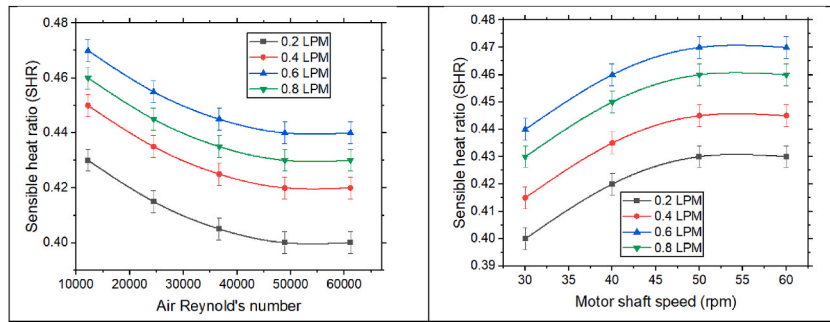


Fig. 9. Change in sensible heat ratio with air Reynold's number & motor shaft speed.

over the high rpm wick, its duration of contact with the moistened surface is shortened, thereby restricting the potential for effective heat transfer. This leads to a reduced temperature differential, resulting in a decline in the sensible heat of the air or attaining a steady state, even as the airflow rate intensifies. Moreover, the sharp increase in the airflow accelerates the rate of evaporation, which predominantly augments the latent heat component (associated with moisture addition) rather than the sensible heat (related to temperature change).

The latent heat ratio is illustrated in Fig. 10, expressed as the proportion of latent heat to total heat. Latent heat itself is given by the product of the air's mass flow rate & change in enthalpy. There are multiple factors contributing to the increase in enthalpy change with the air's Reynolds number. As the air flow rate escalates, so too does the rate of evaporation, accompanied by an enhanced cooling effect. This results in a reduction of the total energy or enthalpy at the exit. The enthalpy drop continues to increase until it reaches a higher air velocity or flow rate. Concurrently, latent heat rises steadily. With increasing air velocity, heat transfer intensifies to substitute warm air with cooler air, indicative of the higher latent heat necessary for the phase transition. The increase in latent heat signifies an augmentation in molecular diffusion, which in turn enhances the evaporation rate. At a flow rate of 0.2 LPM, the latent heat ratio improves by 5.66 % as the air's Reynolds number surges from 12,223 to 61,114.

As packing rotation speed increases, humidification effectiveness declines due to reduced evaporation efficiency, leading to lower latent heat transfer. Higher speeds limit water-air contact time, decreasing the thermal energy absorbed during phase change. In contrast, lower water flow rates enhance evaporation by allowing more moisture absorption and maintaining higher wick surface temperatures, resulting in a higher latent heat ratio. Overall, the latent heat ratio decreases by 5 % with increased motor speed.

#### 5.1.6. Energy consumption

Fig. 11 gives the total energy consumption by the unit by considering the blower, pump and the motor that rotates the wick at a required rpm. The power consumed by the pump is maintained constant, whereas the blower and the motor power consumption are varied, which is controlled using a regulator. The power consumption of the humidifier escalates in tandem with increased blower velocity and rotating motor speed, owing to the heightened mechanical and aerodynamic demands imposed on the system. As the blower velocity intensifies, the fan or blower must exert greater effort to propel a larger volume of air through the system, necessitating additional energy to surmount elevated air resistance and sustain the desired airflow. Likewise, as the rotational speed of the motor increases, the packing material spins at a higher rate, requiring more energy to counteract frictional forces and rotational inertia. Furthermore, elevated speeds often exacerbate mechanical losses and inefficiencies, further amplifying power consumption. Collectively, these factors culminate in a proportional increase in the overall energy required for operating the humidifier at higher blower velocities and motor speeds. As air Reynolds' number increased from 12,223 to 61,114, energy consumption increased by 5.95 %, and at higher air Reynolds' numbers, when motor speed increased from 30 to 90 rpm, the power consumption increased by 82.24 %.

A suction blower is centrally positioned to draw air from both sides of the unit, where it interacts with the wick. The air is drawn in

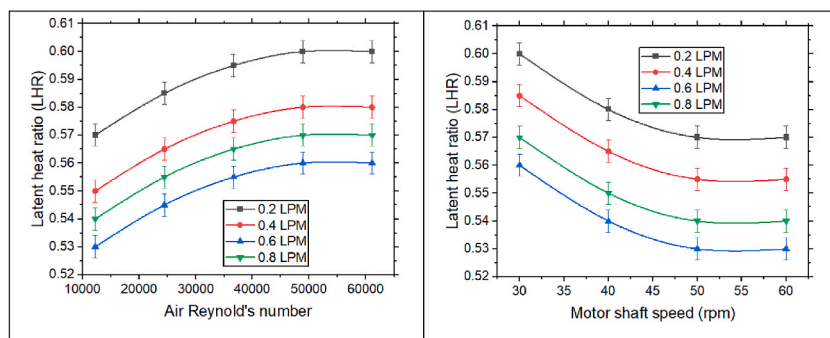


Fig. 10. Change in latent heat ratio with air Reynold's number & motor shaft speed.

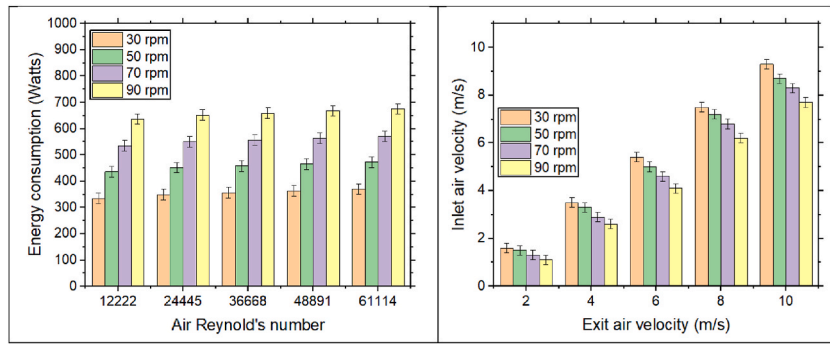


Fig. 11. Energy consumption rate & velocity variation with air Reynold's number.

at varying velocities of 2, 4, 6, 8, and 10 m/s, which correspond to Reynolds numbers ranging from 12,223 to 61,114. Additionally, the motor shaft rotates between 30 and 90 rpm. As the motor speed increases, the inlet air velocity decreases, a pattern consistent across all air velocities drawn in by the blower. As the motor speed increases, the packing material rotates faster, generating stronger centrifugal forces that distribute water more evenly across the surface. As the power consumption of a rotary wick humidifier increases, its overall operating cost rises accordingly due to greater electricity usage. Key components like the motor that drives the rotating drum and any built-in fan consume more energy when run at higher speeds or for extended periods. This elevated power demand leads to increased electricity expenses, particularly in areas with high utility rates.

This enhanced water dispersion increases airflow resistance, as the air must pass through a denser and more turbulent water film. Consequently, the airflow experiences higher drag, reducing the effective inlet air velocity, even though the motor speed has increased. Furthermore, at higher motor speeds, the system may encounter imbalances or inefficiencies in air distribution, such as localized blockages or irregular airflow patterns, which further limit the inlet air velocity. The increased mechanical energy required to maintain higher motor speeds may also divert power from the blower, impeding its capacity to maintain the desired airflow. As a result, despite motor speed rise, the inlet air velocity tends to decrease due to these combined aerodynamic and mechanical factors. For the higher exit velocity, the inlet velocity dropped by 17.20 % when the motor shaft speed rose from 30 to 90 rpm.

## 5.2. Performance parameter comparison between stationary and rotating wick

This section compares stationary and rotary wick packings. Based on the previous discussion, it was found that a motor shaft speed of 70 rpm & water flow rate of 0.6 LPM produced the best results. A motor speed of 0 rpm is considered stationary, while 70 rpm represents the rotating wick humidifier with the optimal flow rate of water of 0.6 LPM.

### 5.2.1. Change in DBT & specific humidity

Fig. 12 depicts the variation in DBT & specific humidity changes relative to the air Reynolds number. Compared to static-type humidifiers, rotary packing ensures more uniform water dispersion across its surface, enhancing evaporation efficiency by evenly distributing water and maximizing the exposed surface area. This increased vaporization absorbs more heat from the air, resulting in a more significant change in DBT. The dynamic motion of the rotary packing drives higher evaporation rates, creating a stronger cooling effect and causing a greater drop in DBT than stationary packing. In stationary packing, the fixed position of the wick restricts water exposure and surface interaction, limiting both cooling and evaporation. As air flow rate rises, cooling effect & vaporization diminish due to the wick drying out more rapidly. This drawback is effectively addressed in rotary packing, where the wick maintains constant wettability. The rotary motion ensures continuous contact between the air & fresh water, enabling sustained evaporation & optimizing

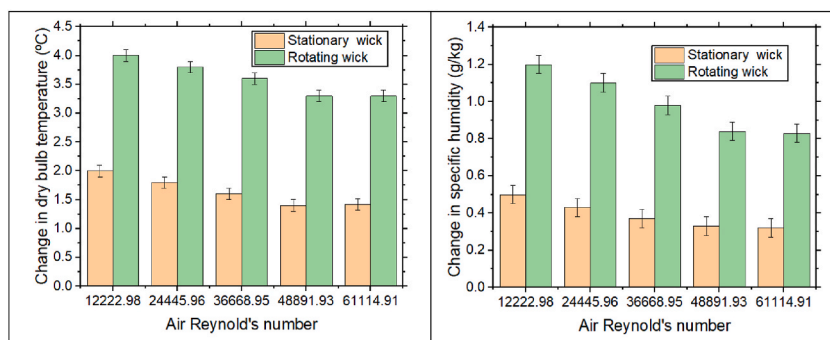


Fig. 12. Change in DBT & Specific humidity (Stationary vs Rotary Packing Wick).

humidification process. At lower Reynolds numbers, change in DBT and specific humidity is observed. Compared to a stationary wick, the rotary wick achieves a 100 % greater change in DBT and a 140 % higher change in specific humidity, demonstrating its superior performance.

### 5.2.2. Change in COP and mass transfer coefficient

Fig. 13 demonstrates the relationship between COP, mass transfer coefficient & air Reynolds number, highlighting the differences between static and dynamic (rotary) packings. Rotary packing ensures uniform water dispersion, consistently wetting the wick and maximizing the surface area exposed to air. This enhanced air-water interaction significantly improves both heat & mass transfer, leading to higher COP & mass transfer coefficient values. The centrifugal effect of the rotary system promotes even water distribution, increasing the evaporation rate and cooling effect, which further elevates the mass transfer coefficient and COP. The continuous renewal of the water film on the surface facilitates the conversion of sensible heat into latent heat, generating water particles carried by the air and reducing air temperature to enhance the cooling effect. In contrast, static packing relies on a fixed interaction zone, which can become less efficient over time as the water film deteriorates. Rotary packing, however, creates a more open and uniform airflow path, minimizing resistance and improving air circulation. This results in superior heat and mass transfer efficiency. Static packing's rigid structure often leads to uneven airflow or blockages, impairing its performance. While the static wick humidifier consumes less energy, the rotary humidifier delivers a significantly greater cooling effect, resulting in a higher COP. Specifically, the COP and mass transfer coefficient of the rotary wick humidifier are 231.82 % and 310.82 % higher, respectively, compared to those of the static packing for higher air Reynold's number. This underscores the superior efficiency and performance of rotary systems in humidification and cooling applications.

### 5.2.3. Change in SHR and LHR

Fig. 14 presents the relationship between the sensible heat ratio (SHR) and latent heat ratio (LHR) as a function of air Reynolds number, contrasting stationary and rotary wicks. With a rise in air Reynolds number, sensible heat ratio diminishes, whereas the latent heat ratio exhibits an upward trend. Dynamic wick packing, as observed in rotary humidifiers, continuously shifts and redistributes water across the packing surface, thereby enhancing the dispersion of water. This perpetual motion improves the exposure of air to fresh, wet surfaces, which in turn accelerates the evaporation process. As evaporation rates rise in such a dynamic system, a greater proportion of the energy is dedicated to latent heat—the energy required for the transition from liquid to vapor—rather than to sensible heat, which typically raises air temperature. Owing to the increased evaporation rate facilitated by dynamic packing, more moisture is absorbed by air, resulting in a higher latent heat component and a reduced sensible heat ratio compared to static systems. For the lower Reynold's number, static wick gave 14.89 % higher sensible heat ratio whereas for the higher Reynold's number, the rotary wick gave 16.667 % higher latent heat ratio compared to the static packing. By comparing the static and dynamic wick packing, the maximum performances are tabulated in Table 3.

The dynamic wick humidifier typically demonstrates higher values in temperature change, specific humidity, mass transfer coefficient, and coefficient of performance (COP) compared to the static wick humidifier, primarily due to its continuous rotation mechanism. The rotating wick continually exposes fresh, water-saturated surfaces to the air, significantly enhancing the evaporation rate. This results in a greater increase in specific humidity and a more noticeable drop in air temperature, owing to the cooling effect of evaporation. The improved evaporation process also leads to a higher mass transfer coefficient, indicating more efficient moisture exchange between the wick and the surrounding air. Additionally, the system achieves higher humidification efficiency with relatively low energy input, resulting in better COP and overall energy performance. In contrast, the static wick humidifier may experience uneven saturation and reduced air-wick interaction, which limits its effectiveness.

### 5.3. Psychrometric representation

Fig. 15 presents the psychrometric representation of the air exiting the unit. For a motor shaft speed of 70 RPM, the air velocity ranges from 2 to 10 m/s, corresponding to Reynolds numbers between 12,223 and 61,114. The exiting air is observed to have varying

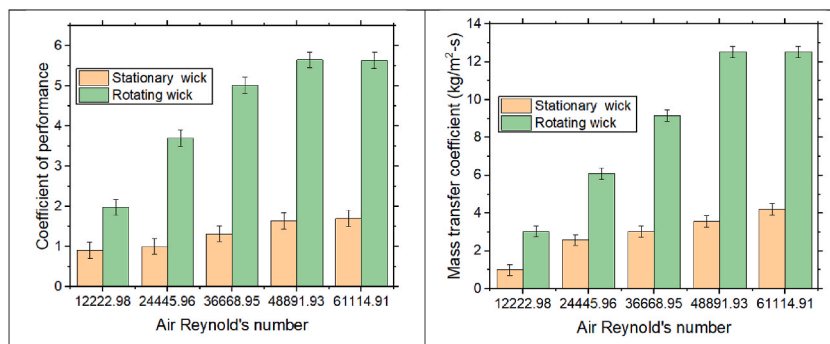


Fig. 13. COP and mass transfer coefficient (Stationary vs Rotary Packing Wick).

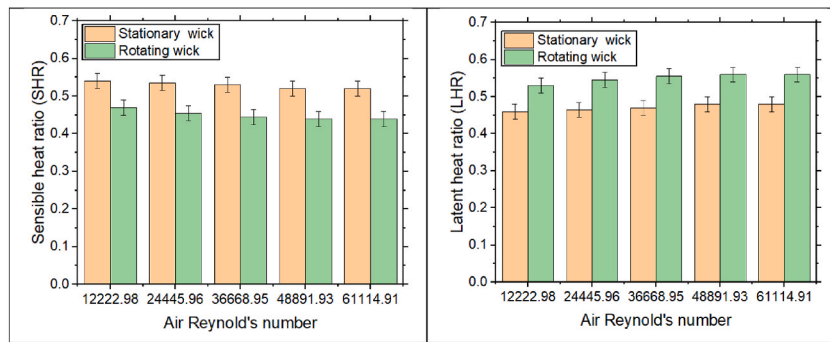


Fig. 14. SHR and LHR (Stationary vs Rotary Packing Wick).

Table 3

Performances with respect to static and dynamic wick packing.

Sl.No.	Performance parameter	Static wick	Dynamic wick	Remarks
1.	Change in temperature (°C)	2	4	Lower air Reynold's number yielded higher change in temperature.
2.	Specific humidity change (g/kg)	0.5	1.2	Lower air Reynold's number yielded higher specific humidity change.
3.	Coefficient of performance	1.7	5.64	Higher air Reynold's number yielded higher COP.
4.	Mass transfer coefficient (kg/m <sup>2</sup> -s)	4.21	12.53	Higher air Reynold's number yielded higher MTC.
5.	Sensible heat ratio	0.54	0.47	Static packing yielded higher results.
6.	Latent heat ratio	0.48	0.56	Higher air Reynold's number yielded higher LHR.

dry bulb temperatures and relative humidity levels. Notably, the exit conditions fall within the thermal comfort range, with relative humidity between 40 % and 60 % and dry bulb temperatures ranging from 22 °C to 27 °C.

## 6. Comparison with existing literature

The output performance parameters of the current rotary wick humidifier are compared with those of the literature, where the performances, such as change in dry bulb temperature & coefficient of performance, were compared. The details are compared and found to be consistent with results obtained in the literature. Comparative analyses are presented in Table 4.

In a rotary wick humidifier, increasing the motor shaft speed from 30 to 90 RPM enhances water evaporation by increasing surface exposure and airflow interaction. However, this also results in an 82.24 % increase in energy consumption due to the higher

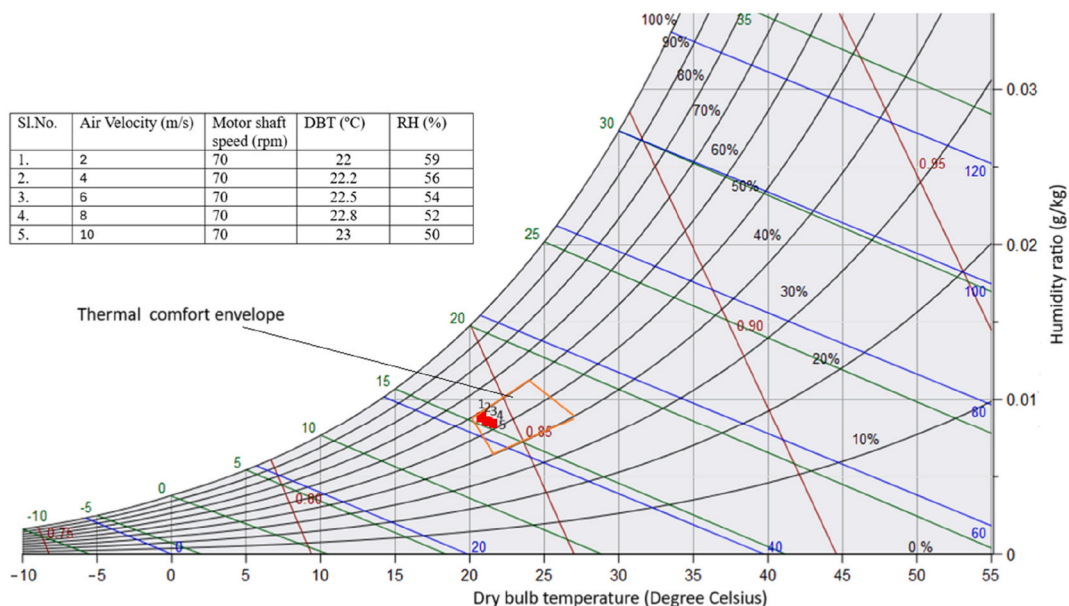


Fig. 15. Psychrometric representation of the outlet air.

mechanical load, increased friction, and greater current draw at higher speeds. This nonlinear relationship highlights the importance of balancing performance with energy efficiency. The current system achieved a coefficient of performance (COP) of 5.65. These results were compared with those of Salins et al. [13], where increasing the motor speed from 50 to 200 RPM led to a 44.54 % increase in power consumption, yielding a COP of 5 and an evaporation rate of 0.55 g/s. Similarly, Kumar et al. [14] observed that increasing the motor speed from 6 to 26 RPM raised power consumption and resulted in a COP of 1.42. Compared to these studies, the present system demonstrates superior performance.

The rotary wick humidifier offers strong potential for scalability and real-life applications due to its simple, modular, and energy-efficient design. Its use of low-cost, readily available components makes it ideal for mass production and deployment in both small and large-scale settings. The system's capacity can be easily scaled by increasing the wick area or adding additional units, allowing it to serve larger spaces with minimal energy consumption. Its quiet operation and low maintenance requirements make it particularly suitable for integration into smart buildings and a wide range of environments. Real-life applications span various sectors: in residential settings, it effectively improves indoor air quality, particularly in dry climates; in greenhouses, it maintains optimal humidity for plant health with minimal water waste; in museums and archives, it protects sensitive materials by regulating humidity; in healthcare facilities, it supports sterile conditions and enhances patient comfort; in offices and commercial buildings, it improves occupant well-being and protects wooden furnishings.

## 7. Conclusions

The present study investigated the performance characteristics of a rotary wick-based evaporative cooling system under varying conditions of air Reynolds number, motor shaft speed, and water flow rate. Based on the experimental results, the following conclusions were drawn.

1. Best performance was achieved at a motor shaft speed of 70 rpm and water flow rate of 0.6 LPM, ensuring continuous wick wetting through gravity and capillarity, and enhancing air–water interaction.
2. At  $Re = 12,223$ , dry bulb temperature rose by 4 °C and specific humidity by 1.2 g/kg, attributed to increased contact time and thicker boundary layers.
3. Increasing air velocity improved cooling with minimal added power, yielding a peak COP of 5.65.
4. Higher airflow boosted evaporation and diffusion, with a maximum mass transfer coefficient of 12.54 kg/m<sup>2</sup>·s. With rising  $Re$ , latent heat absorption improved; at 0.2 LPM, a 5.66 % increase in latent heat ratio was observed from  $Re$  12,223 to 61,114.
5. Energy usage rose by 5.95 % with increasing  $Re$ , while motor speed increased from 30 to 90 rpm, leading to an 82.24 % rise in power consumption.
6. The rotary wick outperformed the static wick, achieving double the DBT reduction and 140 % higher humidity gain due to enhanced centrifugal water distribution.
7. At lower  $Re$ , the static wick favored sensible heat (14.89 % higher), while the rotary wick showed superior latent heat gain (16.67 %) at higher  $Re$ .

Wick-based evaporative cooling systems offer energy-efficient, low-maintenance, and environmentally friendly cooling by utilizing capillary-driven water flow and enhanced evaporation. They consume significantly less power than conventional air conditioning, making them cost-effective and ideal for use in arid regions. Their simple, compact design allows easy integration into various applications, especially in large rooms or buildings. Relying solely on water, they emit no harmful substances, aligning with SDG 7 (Affordable and Clean Energy) and SDG 13 (Climate Action). Overall, the wick humidifier emerges as a sustainable and economical solution for maintaining thermal comfort.

## 8. Novelty, limitations, and future scope

The rotary wick humidifier presents a novel and energy-efficient solution for indoor air management, featuring a dynamic operation mechanism with a rotating wick system that significantly enhances air–water interaction and humidification efficiency over conventional stationary designs. Its design leverages both gravity and capillary action to maintain consistent moisture distribution, leading to superior evaporation and notable improvements in dry bulb temperature reduction and specific humidity increase. With a high coefficient of performance (COP), the system stands out as an energy-efficient option for cooling and humidification. In practical building applications, this humidifier supports improved indoor air quality by maintaining optimal humidity levels (40–60 %), which helps reduce dust, allergens, and airborne pathogens. It also contributes to energy savings by lowering HVAC load, enhances occupant comfort by alleviating issues caused by dry air, operates silently—making it ideal for quiet environments—and promotes sustainability through the use of biodegradable wick materials, aligning with modern green building practices.

The rotary wick humidifier faces some limitations, including potential durability issues with wick materials due to mineral buildup or mold, requiring regular maintenance or replacement. Its effectiveness decreases in high-humidity environments and may be insufficient in very dry or large spaces without multiple units. Additionally, scaling up for industrial use could demand design changes, increased water supply, and larger wick areas, potentially reducing system compactness and efficiency.

The rotary wick humidifier offers strong potential for future enhancements in efficiency, durability, and adaptability. Improved wick materials—antimicrobial and mineral-resistant—could reduce maintenance and extend lifespan. Integrating smart technologies like sensors and IoT would enable real-time humidity control and boost energy efficiency. Future research should focus on performance



**Table 4**

Validation of the current result with other humidifier units.

Sl. No	Authors	Type of system studied	Experimental condition	$\Delta$ DBT (°C)	COP
1.	Present study	Wick type rotary humidifier	Air Reynolds number: 12,223 to 61,114 Water flow rate: 0.2 to 0.8 LPM Motor shaft speed: 30–90 rpm. Celdek Packing	5.4	5.64
2.	Salins et al. [13]	Centrifugal humidifier		Air is at 5–9 m/s or mass flow rates of 0.41–0.74 kg/s. Motor speed: 50–200 rpm.	5
3.	Kumar et al. [14]	Celdek packing type dynamic humidifier	Cam shaft speed: 10–26 rpm Velocity of air: 3.1–8.2 m/s	6.2	1.42
4.	Doğramaci et al. [27]	Eucalyptus packing (Static type)	Air flow rate: 0.06–0.08 kg/s	6.4	3.65
5.	Ndukwu et al. [28]	Jute fiber, palm fruit mesocarp fiber & wooden charcoal	Cooling time: 1–9 h	4	8
6.	Al-Zubaydi, and Hong [29],	Plate walls spray type	Water temperature: 19–22 °C Water flow rate: 25–50 g/s	9.5	10

across varied climates and evaluate long-term cost-effectiveness and environmental impact to support its development as a scalable, eco-friendly solution.

## Nomenclature:

**Abbreviations:**

MTC	Mass transfer coefficient
PVC	Polyvinyl chloride
MH	Membrane Humidifier
CIEC	Counter-flow Indirect Evaporative Cooler
RIEC	Rotary Indirect Evaporative Cooler
AC	Air conditioning
VCR	Vapor compression refrigeration
AV	Air Velocity
CE	Cooling effect
COP	Coefficient of performance
DBT	Dry bulb temperature
WBT	Wet bulb temperature
ER	Evaporation Rate
LPM	Liter per minute
RH	Relative Humidity
RSS	Root Sum of Squares
WFR	Water flow rate
SHR	Sensible heat ratio
LHR	Latent heat ratio

**Variables/Parameters:**

$W_{pump}$	Power utilized by pump, W
$\dot{W}_{Blower}$	Power utilized by blower, W
$\dot{W}_{Motor}$	Power utilized by blower, W
$\dot{m}_a$	Flow rate of air, kg/s
$\dot{m}_w$	Rate of evaporation, kg/s
$W_1$	Humidity ratio at inlet, kg/kg
$W_2$	Humidity ratio at outlet, kg/kg
$\Delta W$	Specific humidity change, kg/kg
$\dot{Q}_c$	Sensible heat transfer rate, W
$\dot{Q}_L$	Latent heat transfer rate, W
$\dot{Q}$	Total heat transfer rate, W
$\eta_H$	Humidification efficiency, %
$T_1$	Dry bulb temperature at inlet, °C
$T_2$	Dry bulb temperature at outlet, °C
$h_1$	Enthalpy at inlet, J/kg
$h_2$	Enthalpy at outlet, J/kg
$T_w$	Wet bulb temperature, °C
$C_p$	Specific heat of the air, J/kg°C
$V$	Velocity of air, m/s
$R$	Dependent variable
$X$	Independent variable
$Y$	Uncertainty intervals
$G$	Function
$Y_G$	Total uncertainty

(continued on next page)

(continued)

$\frac{W_R}{\partial(COP)}$	Overall uncertainty
$\frac{COP}{\partial(K)}$	Uncertainty present in COP
$\frac{SHR}{\partial(LHR)}$	Uncertainty present in Mass transfer coefficient
$\frac{LHR}{\partial(LHR)}$	Uncertainty present in sensible heat ratio
$\frac{LHR}{\partial(LHR)}$	Uncertainty present in latent heat ratio
<b>Subscripts:</b>	
1	Inlet
2	Outlet
a	Air
W	Water
C	Cooling or sensible
H	Humidification
W	Wet Bulb
P	Pressure, Pa
L	Latent
<b>Greek Letters:</b>	
$\eta$	Efficiency, %
$\partial$ and $\Delta$	Change

### CRediT authorship contribution statement

**Sampath Suranjan Salins:** Writing – original draft, Investigation, Conceptualization. **H.K. Sachidananda:** Methodology. **Abdulla Abdul Jaleel:** Data curation. **Moin Alam:** Data curation. **Jaya Jatin Bhavesh Podugu:** Data curation. **Shiva Kumar:** Supervision, Methodology. **Sawan Shetty:** Validation.

### Ethical approval

All actions, recommendations, and decisions in this research are made solely based on merit and integrity, with strict adherence to all relevant standards throughout the study.

### Consent to publish declaration

Consent to publish this work was obtained from all individual participants included in the study.

### Information on funding

Authors received funding from MAHE Dubai university.  
Number: R&DP/MAHE DUBAI/RL-05/2025.

### Declaration of competing interest

There is no conflict of interest among authors for this manuscript.

### Acknowledgement

This project was conducted at the SOEIT MAHE Dubai Laboratory. The authors wish to express their gratitude for the support provided by the organization.

### Appendix 1

Using equation (6) the uncertainties present in the performance parameters are determined. The uncertainty present while measuring the COP is shown in (7).

$$COP = \frac{\dot{Q}_c}{(\dot{W}_{motor} + \dot{W}_{pump} + \dot{W}_{blower})}$$

$$\frac{\partial(COP)}{COP} = \sqrt{\left(\frac{\partial \dot{Q}_c}{\dot{Q}_c}\right)^2 + \left(-\frac{\partial \dot{W}_{pump}}{\dot{W}_{pump}}\right)^2 + \left(-\frac{\partial \dot{W}_{motor}}{\dot{W}_{motor}}\right)^2 + \left(-\frac{\partial \dot{W}_{blower}}{\dot{W}_{blower}}\right)^2} \quad (7)$$

The error present while measuring the MTC is given by equation (8). It is a function of evaporation rate, Surface area & change in

specific humidity.

$$K = \frac{\dot{m}_w}{A \Delta W}$$

$$\frac{\partial(K)}{K} = \sqrt{\left(\frac{\partial \dot{m}_w}{\dot{m}_w}\right)^2 + \left(\frac{\partial A}{A}\right)^2 + \left(\frac{\partial \Delta W}{\Delta W}\right)^2} \quad (8)$$

Uncertainty which evaluating sensible heat ratio is given by equation (9)

$$SHR = \frac{\dot{Q}_c}{\dot{Q}} = \frac{\dot{m}_a C_p \Delta T}{\dot{Q}}$$

$$\frac{\partial(SHR)}{SHR} = \sqrt{\left(\frac{\partial \dot{m}_a}{\dot{m}_a}\right)^2 + \left(\frac{\partial C_p}{C_p}\right)^2 + \left(\frac{\partial \Delta T}{\Delta T}\right)^2 + \left(\frac{\partial \dot{Q}}{\dot{Q}}\right)^2} \quad (9)$$

Error present while measuring the latent heat ratio is given by equation (10).

$$LHR = \frac{\dot{Q}_L}{\dot{Q}} = \frac{\dot{m}_a (h_1 - h_2)}{\dot{Q}}$$

$$\frac{\partial(LHR)}{LHR} = \sqrt{\left(\frac{\partial \dot{m}_a}{\dot{m}_a}\right)^2 + \left(\frac{\partial \Delta h}{\Delta h}\right)^2 + \left(\frac{\partial \dot{Q}}{\dot{Q}}\right)^2} \quad (10)$$

## Data availability

Data will be made available on request.

## References

- [1] K. Srithar, R. Venkatesan, M. Rishidev, R. Saravanan, Optimizing humidifier performance by modifying packing material location and thickness, *Desalination Water Treat.* 317 (2024) 100031.
- [2] K. Thanaiah, V. Gumtapure, G.M. Tadesse, Experimental analysis on humidification-dehumidification desalination system using different packing materials with baffle plates, *Therm. Sci. Eng. Prog.* 22 (2021) 100831.
- [3] A.E. Kabeel, M.R. Diab, M.A. Elazab, E.M. El-Said, Solar powered hybrid desalination system using a novel evaporative humidification tower: experimental investigation, *Sol. Energy Mater. Sol. Cell.* 248 (2022) 112012.
- [4] P. Martinez, J. Ruiz, P.J. Martinez, A.S. Kaiser, M.J.A.T.E. Lucas, Experimental study of the energy and exergy performance of a plastic mesh evaporative pad used in air conditioning applications, *Appl. Therm. Eng.* 138 (2018) 675–685.
- [5] S. Suranjan Salins, S.K. Reddy, S. Kumar, Experimental investigation on use of alternative innovative materials for sustainable cooling applications, *Int. J. Sustain. Eng.* 14 (5) (2021) 1207–1217.
- [6] M. Khan, M.A. Antar, A.E. Khalifa, S.M. Zubair, Experimental investigation of air heated bubble column humidification dehumidification desalination system, *Int. J. Energy Res.* 45 (2) (2021) 2610–2628.
- [7] W. Yan, X. Cui, Y. Liu, C. Tian, S.J. Oh, X. Wang, L. Jin, Performance evaluation and parameter sensitivity analysis of a membrane-based evaporative cooler with built-in baffles, *Appl. Therm. Eng.* 208 (2022) 118228.
- [8] S.A. Nada, H.F. Elattar, M.A. Mahmoud, A. Fouda, Performance enhancement and heat and mass transfer characteristics of direct evaporative building free cooling using corrugated cellulose papers, *Energy* 211 (2020) 118678.
- [9] X. Cheng, G. Yang, J. Wu, Recent advances in the optimization of evaporator wicks of vapor chambers: from mechanism to fabrication technologies, *Appl. Therm. Eng.* 188 (2021) 116611.
- [10] B.A. Fenta, A.S. Ahmmmed, M.A. Delele, Evaluation of water flow in cotton yarn and fabric assemblies for capillary evaporative cooling, *Cog. Eng.* 11 (1) (2024) 2328825.
- [11] D. Pandelidis, A. Cichoń, A. Pacak, P. Drag, M. Drag, K. Sierpowski, W. Worek, S. Cetin, Performance analysis of rotary indirect evaporative air coolers, *Energy Convers. Manag.* 244 (2021) 114514.
- [12] J. Choi, H. Han, T.A. Wani, D. Kim, S. Jeon, Rotating evaporator for sustainable urban cooling and electricity generation, *Appl. Therm. Eng.* 259 (2025) 124933.
- [13] S.S. Salins, P.S. Nair, S.K. Reddy, S. Kumar, Experimental investigations of humidification parameters and transient analysis in a rotating centrifugal humidifier, *J. Build. Eng.* 41 (2021) 102770.
- [14] S. Kumar, S.K. Reddy, S.S. Salins, Experimental investigation on the humidification parameters of the reciprocating multistage evaporative Cooler-A novel approach, *Int. J. Therm. Sci.* 177 (2022) 107539.
- [15] Z.G. Yuan, Y.X. Wang, Y.Z. Liu, D. Wang, W.Z. Jiao, P.F. Liang, Research and development of advanced structured packing in a rotating packed bed, *Chin. J. Chem. Eng.* 49 (2022) 178–186.
- [16] S. Kumar, G. Kumar, D.S. Murthy, Experimental investigation on thermal performance characteristics of rotating packed bed, *Exp. Heat Transf.* 36 (3) (2023) 331–343.
- [17] P. Navarro, J. Ruiz, P. Martínez, M. Lucas, Numerical study of an ultrasonic spray atomiser as an evaporative cooler, *Appl. Therm. Eng.* 236 (2024) 121455.
- [18] S. Kumar, S.S. Salins, P.S. Nair, A. Tejero-González, Parametric evaluation of dynamic multistage centrifugal humidifier, *J. Build. Eng.* 62 (2022) 105305.
- [19] K.D. Kim, Y.C. Choi, Numerical simulation on the generation of ultrasound and formation of water fog in the ultrasonic gas atomizer, *Ultrasonics* 102 (2020) 105851.

- [20] G. Kumar, S. Gole, D.S. Murthy, Analysis of thermal performance characteristics of rotating packed beds using response surface methodology, *Appl. Therm. Eng.* 254 (2024) 123884.
- [21] N. Masaeli, E. Afshari, E. Baniasadi, N. Baharlou-Houreh, M.J.A.E. Ghaedamini, Experimental analysis of water transfer and thermal-hydraulic performance of membrane humidifiers with three flow field designs, *Appl. Energy* 336 (2023) 120823.
- [22] S.S. Shinde, N.P. Gulhane, J. Taler, P. Ocloñ, D. Taler, R. de Lieto Vollaro, Analysis of the effect of packing materials (fills) and flow rate on the range and efficiency of a forced draft evaporative cooling tower, *Energies* 16 (14) (2023) 5255.
- [23] K. Harby, F. Al-Amri, An investigation on energy savings of a split air-conditioning using different commercial cooling pad thicknesses and climatic conditions, *Energy* 182 (2019) 321–336.
- [24] A.S. Abdullah, F.A. Essa, Z.M. Omara, M.A. Bek, Performance evaluation of a humidification–dehumidification unit integrated with wick solar stills under different operating conditions, *Desalination* 441 (2018) 52–61.
- [25] D.M. Weragoda, G. Tian, Q. Cai, T. Zhang, K.H. Lo, Numerical investigation of the saturation effect on wick dry-out in a capillary driven evaporative cooling system, *Int. Commun. Heat Mass Tran.* 155 (2024) 107490.
- [26] A. Almaneea, Experimental investigation of using waste materials as cooling pads for evaporative cooling system, *Arabian J. Sci. Eng.* (2025) 1–7.
- [27] P.A. Doğramacı, S. Riffat, G. Gan, D. Aydın, Experimental study of the potential of eucalyptus fibres for evaporative cooling, *Renew. Energy* 131 (2019) 250–260.
- [28] M.C. Ndukwu, M.I. Ibeh, E.C. Ugwu, D.O. Igbojionu, A.A. Ahiakwo, H. Wu, Evaluating coefficient of performance and rate of moisture loss of some biomass humidifiers materials with a developed simple direct stand-alone evaporative cooling system for farmers, *Energy Nexus* 8 (2022) 100146.
- [29] A.Y.T. Al-Zubaydi, G. Hong, Experimental study of a novel water-spraying configuration in indirect evaporative cooling, *Appl. Therm. Eng.* 151 (2019) 283–293.
- [30] R.J. Tripathi, D. Kumar, V.K. Singh, H. Caliskan, H. Hong, Dynamic performance evaluation of novel evaporative cooling systems under variable environmental conditions, *Appl. Therm. Eng.* (2025) 126598.
- [31] R.J. Tripathi, D. Kumar, J. Sarkar, Experimental investigation on a novel multi-vent dry-channel integrated solar-driven indirect evaporative cooler, *Appl. Therm. Eng.* (2025) 125888.
- [32] V.K. Singh, D. Kumar, An experimental investigation and thermo-economic performance analysis of solar desalination system by using nano-enhanced PCM, *Mater. Today Sustain.* 27 (2024) 100884.
- [33] V.K. Singh, D. Kumar, Heat transfer analysis of solar distillation system by incorporating nano-enhanced PCM as thermal energy-storage system, *Heat Transfer* 53 (8) (2024) 4742–4777.